

The Contribution of Millisecond Pulsars to the Galactic Cosmic-Ray Lepton Spectrum

Christo Venter^{a,1}, Andreas Kopp^{a,2}, Alice K Harding^b, Peter L Gonthier^c,
Ingo Büsching^a

^a*Centre for Space Research, North-West University, Potchefstroom Campus, 2520
Potchefstroom, South Africa*

^b*Astrophysics Science Division, NASA Goddard Space Flight Center, Greenbelt, MD
20771, USA*

^c*Hope College, Department of Physics, Holland, MI, USA*

Abstract

Pulsars are believed to be sources of relativistic electrons and positrons. The abundance of detections of γ -ray millisecond pulsars by *Fermi* Large Area Telescope coupled with their light curve characteristics that imply copious pair production in their magnetospheres, motivated us to investigate this old pulsar population as a source of Galactic electrons and positrons and their contribution to the enhancement in cosmic-ray positron flux at GeV energies. We use a population synthesis code to predict the source properties (number, position, and power) of the present-day Galactic millisecond pulsars, taking into account the latest *Fermi* and radio observations to calibrate the model output. Next, we simulate pair cascade spectra from these pulsars using a model that invokes an offset-dipole magnetic field. We assume free escape of the pairs from the pulsar environment. We then compute the cumulative spectrum of transported electrons and positrons at Earth, following their diffusion and energy losses as they propagate through the Galaxy. Our results indicate that the predicted particle flux increases for non-zero offsets of the magnetic polar caps. Comparing our predicted local interstellar spectrum and positron fraction to measurements by *AMS-02*, *PAMELA*, and *Fermi*, we find that millisecond pulsars are only modest contributors at a

¹Email: Christo.Venter@nwu.ac.za

²On leave from Institut für Experimentelle und Angewandte Physik, Christian-Albrechts-Universität zu Kiel, Leibnizstrasse 11, 24118, Kiel, Germany

few tens of GeV, after which this leptonic spectral component cuts off. The positron fraction is therefore only slightly enhanced above 10 GeV relative to a background flux model. This implies that alternative sources such as young, nearby pulsars and supernova remnants should contribute additional primary positrons within the astrophysical scenario.

Keywords: cosmic rays, pulsars, electrons, positrons 96.50.S-, 97.60.-s, 14.60.Cd, 14.60.Cd

1. Introduction

PAMELA was the first experiment to provide firm evidence of a rising positron fraction (PF), defined as $\phi(e^+)/[\phi(e^+) + \phi(e^-)]$, of the local (leptonic) interstellar spectrum above ~ 10 GeV (Adriani et al., 2009). The *Fermi* Large Area Telescope (LAT) has confirmed this result (Ackermann et al., 2012), and *PAMELA* has recently extended the measurement range up to 300 GeV (Adriani et al., 2013). *AMS-02* has now provided a PF measurement in the range $0.5 - 350$ GeV (Aguilar et al., 2013) for 18 months of data, and improved spectra for 30 months of data (Aguilar et al., 2014; Accardo et al., 2014), extending the PF up to 500 GeV and indicating a levelling off of this fraction with energy, as well as finding the PF to be consistent with isotropy.

Positrons are created during inelastic collisions involving cosmic-ray nuclei and intergalactic hydrogen, which produce charged pions that in turn decay into positrons, electrons, and neutrinos. The fraction of such a *secondary* positron component with respect to the total leptonic cosmic-ray spectrum is expected to smoothly decrease³ with energy (e.g., Moskalenko & Strong, 1998). However, the *AMS-02* electron spectrum is softer than the positron flux in the range $20 - 200$ GeV (Aguilar et al., 2014), and the measured PF rises with energy, pointing to nearby sources of *primary* positrons. Moreover, the rising PF can be ascribed to a hardening of the positron spectrum (up to 200 GeV, after which it softens with energy), and not a softening in electron spectrum above 10 GeV.

The purported additional source of primary positrons may be either of astrophysical or dark matter annihilation origin (e.g., Fan et al., 2010; Porter

³This, however, depends on model assumptions, i.e., a concave electron spectrum may lead to a rising PF.

et al., 2011). The first case may include supernovae (e.g., Blasi, 2009; Delahaye et al., 2010), microquasar jets (Gupta & Torres, 2014) pulsar wind nebulae (e.g., Serpico, 2012), mature pulsars (Zhang & Cheng, 2001), and millisecond pulsars (MSPs; Kisaka & Kawanaka, 2012). The detection of a potential anisotropy in lepton flux may be an important discriminator between dark matter vs. pulsar (or supernova remnant) scenarios (Accardo et al., 2014), although this may depend on the number of individual sources that collectively contribute to the cosmic-ray lepton spectrum at Earth.

Alternatively, there have been several attempts to modify the standard Galactic cosmic-ray transport models in order to explain the observed rise in PF with energy purely by secondary positrons originating in the interstellar medium. Shaviv et al. (2009) demonstrated that an inhomogeneous distribution of SNRs, such as a strong concentration in the Galactic spiral arms, may explain the PF shape. Moskalenko (2013) pointed out that the concave shape of the primary electron spectrum of Shaviv et al. (2009) introduces an arguably artificial rise in the PF. Cowsik & Burch (2010) put forward a model that assumes a significant fraction of the boron below 10 GeV is generated through spallation of cosmic-ray nuclei in small regions around the sources; GeV positrons would then almost exclusively be generated through cosmic-ray interactions in the interstellar medium. Moskalenko (2013) noted that such sources should be observable as very bright GeV γ -ray sources with soft spectra, while the diffuse emission would be significantly dimmer than observed. This scenario is also at odds with current estimates of the supernova birth rate. Blum et al. (2013) found an upper bound to the positron flux by neglecting energy losses, arguing that the flattening of the PF seen by *AMS-02* around several hundred GeV is consistent with a purely secondary origin for the positrons. Moskalenko (2013) noted that their arguments imply quite hard injection spectra for primary nuclei, in contradiction to γ -ray observations of SNRs. A very fast escape time for the positrons is furthermore implied, and if this is extrapolated to higher energies, it would lead to a large cosmic-ray anisotropy, which has not been observed.

The presence of γ -ray photons and intense magnetic fields in pulsar magnetospheres facilitate copious electron-positron pair production (Sturrock, 1971; Daugherty & Harding, 1982), making pulsars prime candidate sources of primary Galactic leptons. We previously studied the contribution to the local electron spectrum by the nearby MSP PSR J0437–4715 (assuming a pair-starved potential) as well as Geminga, and found that the latter may contribute significantly, depending on model parameters (Büsching et al.,

2008a). Büsching et al. (2008b) also noted that Geminga and PSR B0656+14 may be the dominant contributors to the local positron flux, and may be responsible for an anisotropy of up to a few percent in this flux component, depending on model parameters. Moskalenko (2013) however notes that to date the pulsar scenario lacks convincing calculations of the number of ejected particles and their spectrum.

In this paper, we carefully assess the contribution of MSPs (excluding those found in the globular clusters) to the cosmic-ray lepton spectrum at Earth, given the large number of *Fermi*-detected Galactic γ -ray MSPs (Abdo et al., 2013), and the fact that their measured light curves imply abundant pair production even for this much older pulsar class (Venter et al., 2009). We use a population synthesis code to predict the source properties (Section 2) and a pair cascade code to find realistic injected pair spectra (Section 3). We next combine inverse Compton (IC) scattering of leptons on the local interstellar radiation field (ISRF; Section 4) and their synchrotron radiation (SR) in the Galactic B -field (Section 5) into an effective loss term (Section 6), and use this together with a prescription for particle diffusion when solving a transport equation (Section 7) to calculate the spectra at Earth (Section 8). We discuss our results Section 9. More details will be provided in Venter et al. (submitted for publication).

2. Present-Day Distribution of Galactic MSPs

We implement the results of a new study by Gonthier et al. (2015) of the population synthesis of radio and γ -ray MSPs that lead to the present-day distribution of MSPs. This distribution of MSPs is assumed to be an equilibrated one within the Galaxy. Its evolution has been described in Section 3 of Story et al. (2007, hereafter SGH), where the radial (ρ in cylindrical coordinates) distribution was assumed to be that of the work of Paczyński (1990), with a radial scaling of 4.5 kpc and a scale height of 200 pc instead of 75 pc used in that work. In addition, we implement the supernova kick velocity model of Hobbs et al. (2005) using a Maxwellian distribution with a width of 70 km s^{-1} (resulting in an average of speed of 110 km s^{-1}). The Galaxy is seeded with MSPs treated as point particles with ages going back to the past 12 Gyr assuming a constant birth rate of 4.5×10^{-4} MSPs per century as obtained in SGH. The MSPs are evolved in the Galactic potential from their birth location to the present time. Enough stars were evolved to obtain an equilibrium distribution of the present-day spatial distribution of MSPs.

We assume that MSPs are “born” on the spin-up line with initial period P_0 dependent on magnetic field, which we assume does not decay with time. We use a power-law distribution for the B -fields, similar to SGH. The simulation prefers a power-law distribution of periods $P(B_8)$, with $B_8 = B_0/(10^8 \text{ G})$, and with an index α_B (as in SGH). We achieve improved agreement with the new simulation with an index of $\alpha_B = -1.3$ (as opposed to the value $\alpha_B = -1$ used in SGH).

We assume a distribution of mass accretion birth lines from the Eddington critical mass accretion rate to about 10^{-3} of this value following the study by [Lamb & Yu \(2005\)](#). We parameterise the mass accretion rates with a line in the $\dot{P} - P$ diagram as was done in Eq. (5) of SGH.

Force-free electrodynamic solutions for the magnetosphere ([Spitkovsky, 2006](#)) led to the following description of the pulsar spin-down power L_{sd} :

$$L_{\text{sd}} \sim \frac{2\mu^2\Omega^4}{3c^3} (1 + \sin^2 \alpha), \quad (1)$$

where μ is the magnetic dipole moment, Ω is the rotational angular velocity, c is the speed of light, and α is the magnetic inclination angle relative to the pulsar’s rotational axis. This is similar to the results of [Li et al. \(2012\)](#) for resistive magnetospheres and those of [Contopoulos et al. \(2014\)](#) for force-free magnetospheres with current layers that depart from these ideal conditions. Equating L_{sd} to the rate of rotational energy loss, solving for B_0 , and integrating this result over the age t of the pulsar provides the present-day period P from the pulsar’s birth period P_0 :

$$P^2 = P_0^2 + \frac{4\pi^2 R^6}{3c^3 I} (1 + \sin^2 \alpha) B_0^2 t. \quad (2)$$

We assume $R = 12 \text{ km}$ and $M = 1.6 M_\odot$, where M_\odot is the mass of the Sun. We use a moment of inertia of $I = 1.7 \times 10^{45} \text{ g cm}^2$ ([Pierbattista et al., 2012](#)).

Our population synthesis model has been calibrated against *Fermi* LAT data as well as those from a dozen radio surveys. Details, as well as comparison of simulated and observed radio and γ -ray pulsar properties (e.g., histograms of period, period derivative, surface magnetic field, characteristic age, and distance) will appear in our follow-up paper ([Venter et al., submitted for publication](#)), as well as in [Gonthier et al. \(2015\)](#).

3. Electron-Positron Pair Spectra

We calculate the source spectra using a code that follows the development of a polar cap electron-positron pair cascade in the pulsar magnetosphere (details of the calculation can be found in [Harding & Muslimov, 2011](#)). The pair cascade is initiated by curvature radiation of electrons accelerated above the polar cap by a parallel electric field, derived assuming space-charge-limited flow (free emission of particles from the neutron star surface). A fraction of the photons undergo magnetic pair attenuation, producing a first-generation pair spectrum which then radiates synchrotron photons that produce further generations of pairs. The total cascade multiplicity (average number of pairs spawned by each primary electron) is a strong function of pulsar period P and surface magnetic field strength B_0 , so that many pulsars with low B -fields and long periods produce either few or no pairs, leading to a pair death line.

The sweepback of magnetic field lines near the light cylinder (where the corotation speed equals the speed of light) as well as non-symmetric currents within the neutron star may cause the magnetic polar caps to be offset from the dipole axis. This may in turn lead to enhanced local electric fields, boosting pair formation, even for pulsars beyond the pair death line for pure dipole fields. We include this effect by using an offset-dipole magnetic field and find pair spectra (Figure 1) that are quite hard, characterised by P , \dot{P} (or equivalently, B_0), and offset parameter ε ([Harding & Muslimov, 2011](#)). From our first-principles cascade simulation, we find that about $\sim 1\%$ of L_{sd} is tapped to generate the pairs.

We used a grid in P and B_0 and interpolated the spectra to find an adequate injection spectrum for each source in the present-day MSP population (Section 2). We used an inclination angle of $\alpha = 45^\circ$, mass $M = 2.15M_\odot$, radius $R = 9.9$ km, and moment of inertia $I = 1.56 \times 10^{45}$ g cm² for all MSPs⁴. We used dipole offsets of $\varepsilon = (0.0, 0.2, 0.6)$ and set $\phi_0 = \pi/2$ (this parameter controls the direction of offset of the polar cap).

⁴We adopted an equation of state with larger M here (and associated smaller I) compared to that used in the population code (Section 2), since some MSPs have measured masses $M \sim 2M_\odot$ ([Demorest et al., 2010](#)), and this enhances pair multiplicity. However, this discrepancy is removed by considering a large range of ε , since the latter simulates a large range of pair multiplicities that would correspond to different equations of state, and thus values of M .

Since MSPs are not surrounded by nebulae that can trap the pairs and degrade their energy before escape, we can assume that the pair spectra emerging from the MSPs are good representations of the intrinsic source spectra. A number of MSPs are in binary systems and a subset of these, the black widows and redbacks, may contain strong interbinary shocks that can further accelerate the pairs. We will neglect the contribution from these sources here, but plan to treat this potentially important component in a future paper (Venter et al., submitted for publication).

4. Interstellar Radiation Field (ISRF)

In order to calculate IC losses suffered by leptons propagating through our Galaxy, one needs to know the spectral and spatial properties of Galactic “background photons” or ISRF. Optical stellar photons as well as infrared (IR) photons that result from scattering, absorption, and re-emission of the stellar photons by dust in the interstellar medium contribute to this field (Porter et al., 2008).

The GALPROP code (Strong & Moskalenko, 1998) includes a detailed ISRF model that incorporates a stellar population model, dust grain abundance and size distribution, as well as the absorption and scattering efficiencies of the latter (see also Moskalenko et al. 2006; Porter et al. 2006, 2008). We find that the ISRF is adequately approximated by three black-body components (optical, IR, and cosmic microwave background or CMB) as shown in Figure 2 (for the Galactic Plane). We will use average photon energy densities to calculate the IC loss rate (see Eq. [13]). One can distinguish between two main spatial regions: the Galactic Plane and the Galactic Halo. For the Plane, we use $U_{\text{optical}} = U_{\text{IR}} = 0.4 \text{ eV cm}^{-3}$, and $U_{\text{CMB}} = 0.23 \text{ eV cm}^{-3}$ (Schlickeiser & Ruppel, 2010), while for the Halo, we use $U_{\text{optical}} = 0.8 \text{ eV cm}^{-3}$, $U_{\text{IR}} = 0.05 \text{ eV cm}^{-3}$, and $U_{\text{CMB}} = 0.23 \text{ eV cm}^{-3}$ (Blies & Schlickeiser, 2012).

5. The Galactic Magnetic Field

We are interested in an average field strength that would determine SR loss rates (Eq. [3]), and not so much in the overall Galactic field structure (which is still under debate). The total field has been estimated to be around $6 \mu\text{G}$, averaged over a distance of 1 kpc around the Sun, using radio SR measurements and equipartition arguments. This number increases to \sim

10 μG closer to the inner Galaxy (see [Beck, 2009](#), and references therein). [Han et al. \(2006\)](#) used a combination of dispersion and rotation measures of over 500 pulsars and found that the regular B -field component⁵ decreases from $\sim 6 \mu\text{G}$ near a Galactocentric distance of 2 kpc to $\sim 1 \mu\text{G}$ near 9 kpc; the value is $\sim 2 \mu\text{G}$ near the Sun (see Figure 11 of [Han et al., 2006](#)). Furthermore, the mean regular field as function of latitude is inferred to vary between $\sim -5 \mu\text{G}$ and $\sim 5 \mu\text{G}$ ([Han et al., 2006](#)). [Orlando & Strong \(2013\)](#) inferred values of $\sim 2 \mu\text{G}$, $\sim 5 \mu\text{G}$, and $\sim 2 \mu\text{G}$ for the local regular, random, and anisotropic field components in the Disc via Galactic SR modelling. It is, however, important to note that the average total field decreases when taking into account its rapid decay with height above the Plane. [Delahaye et al. \(2010, hereafter D10\)](#) therefore argue that the relevant B -field (the square root of the sum of averages of the squares of all field components) to be used in SR calculations may reasonably be $1 - 3 \mu\text{G}$.

6. Total Leptonic Energy Loss Rate

The SR loss rate is given by

$$\dot{E}_{\text{SR}} = \frac{4\sigma_{\text{T}}cU_BE^2}{3(m_ec^2)^2}, \quad (3)$$

with σ_{T} the Thomson cross section, E the lepton energy, and the magnetic energy density

$$U_B = \frac{B^2}{8\pi} = 0.098b_2^2 \text{ eV cm}^{-3} \quad (4)$$

for $b_2 = B/(2.0 \mu\text{G})$. The general expression for the IC loss rate (for target photons of energy density U_i , for the i^{th} blackbody component) may be approximated as (for details, see the appendix of [Schlickeiser & Ruppel, 2010](#))

$$\dot{E}_{\text{IC}} = \frac{4\sigma_{\text{T}}cU_iE^2}{3(m_ec^2)^2} \frac{\gamma_K^2}{\gamma_K^2 + \gamma^2}, \quad (5)$$

with the critical Klein-Nishina Lorentz factor defined as

$$\gamma_K \equiv \frac{3\sqrt{5}m_ec^2}{8\pi k_B T} \approx \frac{0.27m_ec^2}{k_B T}, \quad (6)$$

⁵The Galactic B -field is typically divided into three components: regular, random, and anisotropic ([Beck, 2009](#)).

and m_e the electron mass. If $\gamma \ll \gamma_K$, we recover the well-known expression for the Thomson limit (Blumenthal & Gould, 1970)

$$\dot{E}_{\text{IC}} = \frac{4\sigma_{\text{T}}cU_iE^2}{3(m_e c^2)^2}. \quad (7)$$

The Klein-Nishina correction is only necessary for optical photons, where $\gamma_K \sim 10^5$. The IC loss rate for particles with Lorentz factors above γ_K is severely suppressed. For simplicity, one may choose to neglect this correction, which implies an overestimation of the IC loss rate for particles at the highest energies. This, however, allows the introduction of an effective B -field, $B_{\text{eff}} = qB$, which simulates the effect of adding the IC and SR losses (Blies & Schlickeiser, 2012):

$$\begin{aligned} \dot{E} &= \dot{E}_{\text{SR}} + \dot{E}_{\text{IC}} = \frac{4\sigma_{\text{T}}cE^2}{3(m_e c^2)^2} \left[U_B + \sum_i U_i \right] \\ &= \frac{4\sigma_{\text{T}}cE^2}{3(m_e c^2)^2} U_{\text{eff}} = b_0 E^2, \end{aligned} \quad (8)$$

$$U_{\text{eff}} = U_B(1 + f) = \frac{B_{\text{eff}}^2}{8\pi} = q^2 \frac{B^2}{8\pi}, \quad (9)$$

$$f = \frac{\sum_i U_i}{U_B}, \quad (10)$$

$$q = \sqrt{1 + f}, \quad (11)$$

$$b_0 = \frac{4c}{9} \left(\frac{e}{m_e c^2} \right)^4 B_{\text{eff}}^2 = 1.58 \times 10^{-15} \left(\frac{B_{\text{eff}}}{1 \mu\text{G}} \right)^2. \quad (12)$$

If one considers typical constant average values of $B = 2 - 3 \mu\text{G}$ for the Galactic Plane and $B = 1 \mu\text{G}$ for the Galactic Halo, one ends up with $B_{\text{eff}} \approx 7 \mu\text{G}$ in both cases. This is because the increase in U_{optical} is coupled with the decrease in B as one moves from the Galactic Plane to the Halo. However, to account for the fact that the Thomson loss rate overestimates the true IC loss rate, we will rather use values of $B_{\text{eff}} = 2 \mu\text{G}$ and $B_{\text{eff}} = 5 \mu\text{G}$, which should give a reasonable range for the predictions of cosmic-ray lepton flux from nearby MSPs.

7. Transport Model

We solve a Fokker-Planck-type transport equation

$$\frac{\partial n_e}{\partial t} = \nabla \cdot (\mathcal{K} \cdot \nabla n_e) - \frac{\partial}{\partial E} (\dot{E} n_e) + S, \quad (13)$$

with n_e the lepton density (per energy interval) and E the lepton energy. Also, \mathcal{K} denotes the diffusion tensor and \dot{E} energy losses, while S is the source term. We consider a steady-state case, as well as spatially-independent diffusion (so that \mathcal{K} becomes only a function of energy $\kappa(E)$), assuming a power-law dependence on energy:

$$\kappa(E) = \kappa_0 \left(\frac{E}{E_{\text{norm}}} \right)_{\text{D}}^{\alpha}, \quad (14)$$

and we assume typical values of $\alpha_{\text{D}} = 0.6$, $E_{\text{norm}} = 1$ GeV, and $\kappa_0 = 0.1 \text{ kpc}^2 \text{ Myr}^{-1} \approx 3 \times 10^{28} \text{ cm}^2 \text{ s}^{-1}$ (e.g., [Moskalenko & Strong, 1998](#)). The source term refers to the pair spectra $Q_i(P, B_0, \varepsilon, E)$ of $N \sim 4 \times 10^4$ Galactic MSP sources (i.e., for the i^{th} pulsar in our population, we assign a pair spectrum $Q_i(P, B_0, \varepsilon, E)$, as calculated in Section 3 for the corresponding simulated values of P , B_0 , and ε ; the properties of this population have been calculated in Section 2):

$$S = \sum_i^N Q_i(E) \delta(\mathbf{r} - \mathbf{r}_{0,i}). \quad (15)$$

Here, $\mathbf{r}_{0,i}$ are the source positions. For an infinite system, Eq. (13) is solved by the following Green's function ([Delahaye et al., 2010](#); [Blies & Schlickeiser, 2012](#)):

$$G(\mathbf{r}, \mathbf{r}_0, E, E_0) = \frac{\Theta(E_0 - E)}{\dot{E} (\pi \lambda)^{3/2}} \exp \left(-\frac{|\mathbf{r} - \mathbf{r}_0|^2}{\lambda} \right) \quad (16)$$

with E_0 the particle energy at the source, and the square of the propagation scale characterised by

$$\lambda(E, E_0) \equiv 4 \int_E^{E_0} \frac{\kappa(E')}{b(E')} dE', \quad (17)$$

$$= \lambda_0 \left[\frac{1}{E_0} \left(\frac{E_0}{E_{\text{norm}}} \right)^{\alpha_{\text{D}}} - \frac{1}{E} \left(\frac{E}{E_{\text{norm}}} \right)^{\alpha_{\text{D}}} \right], \quad (18)$$

$$\lambda_0 = \frac{4\kappa_0}{(\alpha_{\text{D}} - 1) b_0}, \quad (19)$$

and $\Theta(E_0 - E)$ the Heaviside function. The latter is used to ensure that $\lambda > 0$. The lepton flux may then be found using

$$\phi_e(\mathbf{r}, E) = \frac{c}{4\pi} \iiint G(\mathbf{r}, \mathbf{r}_0, E, E_0) S dE_0 d^3r_0. \quad (20)$$

While the finite boundary of the Galactic Halo should impact the solution, this effect is not too large for GeV leptons, for which the propagation scale is only a few kpc (D10), and we neglect it here for simplicity. Our results will indicate that our predicted MSP contribution becomes significant above ~ 10 GeV, so that the effect of solar modulation may safely be neglected (Strauss & Potgieter, 2014).

8. Results

Figure 3 indicates the “background” electron and positron fluxes predicted by D10 (we use their secondary positron flux as well as the sum of their secondary electron flux and primary electron flux originating in distant supernova remnants, as indicated in their Figure 14), as well as data from *Fermi* (Ackermann et al., 2012), *PAMELA* (Adriani et al., 2013), and *AMS-02* (Aguilar et al., 2014). We furthermore indicate primary electrons and positrons from MSPs for dipole offsets of $\varepsilon = (0.0, 0.2, 0.6)$ and Galactic B -fields of $B_{\text{eff}} = 2 \mu\text{G}$ and $B_{\text{eff}} = 5 \mu\text{G}$. The various curves are distinguished in the Figure caption.

Figure 4 shows the measured PF (e.g., Accardo et al., 2014) as well as the D10 and (D10 + MSP) contributions. The largest contribution is found in the case of $\varepsilon = 0.6$ and $B = 2 \mu\text{G}$. The contribution is lower for $\varepsilon = 0.6$ and $B_{\text{eff}} = 5 \mu\text{G}$, and negligible for $\varepsilon = 0.0$ and $\varepsilon = 0.2$.

9. Conclusion

The predicted MSP contribution increases for non-zero values of polar cap offset parameter ε . This is expected, since a larger value for the offset of the surface B -field with respect to the non-perturbed magnetic axis leads to an increase in the acceleration potential for some regions in azimuthal phase (and a decrease in others). This in turn results in an enhancement in both the number of particles (since the multiplicity will be higher) as well as the maximum particle source energy. We find that the MSPs make only a modest

contribution to the local cosmic-ray flux at a few tens of GeV, after which this spectral component cuts off.

The effect of different Galactic B -fields is also shown. Increasing B_{eff} leads to an increased energy loss rate $\dot{E}_{\text{SR}}(E) \propto B_{\text{eff}}^2$ and a decrease in particle flux. We will address the effect of including Klein-Nishina corrections to the total loss rate in a future work (Venter et al., submitted for publication). The result should however be in a similar range, while the spectral shape may change somewhat, since the high-energy particles will suffer smaller loss rates and hence have longer survival times.

Although the PF is somewhat enhanced above 10 GeV (also depending on the “background” model for the secondary positron flux), our added MSP component fails to reproduce the high-energy rise for the parameters considered. This implies alternative sources of primary positrons such as young, nearby pulsars or supernova remnants (e.g., Di Mauro et al., 2014).

Kisaka & Kawanaka (2012) suggested that pair-starved MSPs may be responsible for a large peak in the total electron spectrum at 10 – 100 TeV, and that non-pair-starved MSPs with multiplicities of $\sim 2\,000$ may contribute significantly (near 100%) to the PF above 10 GeV. There are, however, a number of differences in our respective approaches. Kisaka & Kawanaka (2012) use fixed values for P and B_0 for all members in their population. They furthermore assumed energy equipartition between the particles and the B -field, which seems to imply a conversion efficiency (from spin-down luminosity to particle power) of $\eta \sim 50\%$, while we find $\eta \sim 1\%$ from our simulations. Their diffusion coefficient is slightly larger than ours, and they assume a lower average Galactic B -field ($B = 1\,\mu\text{G}$) as well as including a Klein-Nishina correction for their IC losses. Finally, they integrate the injected spectra over the age of the MSPs while we follow a steady-state approach. Most if not all of these differences should lead to an enhanced particle flux in their case.

Our population synthesis uses radio survey sensitivity and *Fermi* three-year point source sensitivity maps, normalising to the number of detected radio MSPs from those surveys only, and to the detected γ -ray MSPs in the 2nd *Fermi* pulsar catalogue, all of which are radio-loud. The MSPs discovered in radio followup observations of unidentified *Fermi* sources are included in our simulated population of MSPs not detected by surveys but detected by *Fermi* as point sources. However, it is possible that there is a contribution to the cosmic-ray flux from MSPs in binary systems (e.g., black widows or redbacks) very close to Earth that, due to difficulty of radio detection in these

eclipsing and/or obscured systems, have not been identified. These systems may further accelerate the electron-positron pairs in the strong interbinary shocks, and we will investigate this potentially important contribution in a future paper. We will lastly also consider the effect of different assumptions for the magnitude of the spatial diffusion coefficient ([Venter et al., submitted for publication](#)).

References

- Abdo, A.A. et al., The second *Fermi* Large Area Telescope catalog of gamma-ray pulsars, *ApJS*, 208, 17-75, 2013.
- Accardo, L. et al., High statistics measurement of the positron fraction in primary cosmic rays of 0.5–500 GeV with the Alpha Magnetic Spectrometer on the International Space Station, *Phys. Rev. Lett.*, 113, 121101, 2014.
- Ackermann, M. et al., Measurement of separate cosmic-ray electron and positron spectra with the *Fermi* Large Area Telescope, *Phys. Rev. Lett.*, 108, 011103, 2012.
- Adriani, O. et al., An anomalous positron abundance in cosmic rays with energies 1.5–100 GeV, *Nature*, 458, 607-609, 2009.
- Adriani, O. et al., Cosmic-ray positron energy spectrum measured by *PAMELA*, *Phys. Rev. Lett.*, 111, 081102, 2013.
- Aguilar, M. et al., First result from the Alpha Magnetic Spectrometer on the International Space Station: precision measurement of the positron fraction in primary cosmic rays of 0.5–350 GeV, *Phys. Rev. Lett.*, 110, 141102, 2013.
- Aguilar, M. et al., Electron and positron fluxes in primary cosmic rays measured with the Alpha Magnetic Spectrometer on the International Space Station, *Phys. Rev. Lett.*, 113, 121102, 2014.
- Beck, R., Galactic and extragalactic magnetic fields - a concise review, *Astrophys. Space Sci. Trans.*, 5, 43-47, 2009.
- Blasi, P., Origin of the positron excess in cosmic rays, *Phys. Rev. Lett.*, 103, 051104, 2009.

- Blies, P., & Schlickeiser, R., The influence of Klein-Nishina steps on the spatial diffusion of Galactic cosmic-ray electrons, *ApJ*, 751, 71-77, 2012.
- Blum, K., Katz, B., & Waxman, E., AMS-02 Results Support the Secondary Origin of Cosmic Ray Positrons, *PRL*, 111, 211101, 2013.
- Blumenthal, G.R., & Gould, R.J., Bremsstrahlung, synchrotron radiation, and Compton scattering of high-energy electrons traversing dilute gases, *Rev. Mod. Phys.*, 42, 237-271, 1970.
- Büsching, I., Venter, C., & de Jager, O.C., Contributions from nearby pulsars to the local cosmic ray electron spectrum, *Adv. Space Res.*, 42, 497-503, 2008a.
- Büsching, I., de Jager, O.C., Potgieter, M.S., & Venter, C., A cosmic-ray positron anisotropy due to two middle-aged, nearby pulsars?, *ApJ*, 678, L39-L42, 2008b.
- Contopoulos, I., Kalapotharakos, C., & Kazanas, D., A new standard pulsar magnetosphere, *ApJ*, 781, 46-50, 2014.
- Cowsik, R., & Burch, B., Positron fraction in cosmic rays and models of cosmic-ray propagation, *Phys. Rev. D*, 82, 023009, 2010.
- Daugherty, J.K. & Harding, A.K., Electromagnetic cascades in pulsars, *ApJ*, 252, 337-347, 1982.
- Delahaye, T., Laval, J., Lineros, R., Donato, F., & Fornengo, N., Galactic electrons and positrons at the earth: new estimate of the primary and secondary fluxes, *A&A*, 524, A51, 2010 (D10).
- Demorest, P.B., Pennucci, T., Ransom, S.M., Roberts, M.S.E., & Hessels, J.W.T., A two-solar-mass neutron star measured using Shapiro delay, *Nature*, 467, 1081-1083, 2010.
- Di Mauro, M., Donato, F., Fornengo, N., Lineros, R., & Vittino, A., Interpretation of AMS-02 electrons and positrons data, *JCAP*, 4, 6-39
- Fan, Y.-Z., Zhang, B., & Chang, J., Electron/positron excesses in the cosmic ray spectrum and possible interpretations, *Int. J. Mod. Phys. D*, 19, 2011-2058, 2010.

- Gonthier, P.L. et al., Population synthesis of radio and gamma-ray millisecond pulsars from the Galactic disk, in prep.
- Gupta, N. & Torres, D.F., $p\gamma$ interactions in Galactic jets as a plausible origin of the positron excess, MNRAS, 441, 3122-3126, 2014.
- Han, J.L., Manchester, R.N., Lyne, A.G., Qiao, G.J., & van Straten, W., Pulsar rotation measures and the large-scale structure of the Galactic magnetic field, ApJ, 642, 868-881, 2006.
- Harding, A.K., & Muslimov, A.G., Pulsar pair cascades in magnetic fields with offset polar caps, ApJ, 743, 181-196, 2011.
- Hobbs, G., Lorimer, D.R., Lyne, A.G., & Kramer, M., A statistical study of 233 pulsar proper motions, MNRAS, 360, 974-992, 2005.
- Kisaka, S., & Kawanaka, N., TeV cosmic-ray electrons from millisecond pulsars, MNRAS, 421, 3543-3549, 2012.
- Lamb, F., & Yu, W., Spin rates and magnetic fields of millisecond pulsars, in Binary Radio Pulsars, ASP Conf. Ser., ed. F.A. Rasio & I.H. Stairs, 328, 299-310, 2005.
- Li, J., Spitkovsky, A., & Tchekhovskoy, A., Resistive solutions for pulsar magnetospheres, ApJ, 746, 60-71, 2012.
- Maurin, D., Melot, F., & Taillet, R., A database of charged cosmic rays, A&A, 569, A32, 2014.
- Moskalenko, I.V., & Strong, A.W., Production and propagation of cosmic-ray positrons and electrons, ApJ, 493, 694-707, 1998.
- Moskalenko, I.V., Porter, T.A., & Strong, A.W., Attenuation of very high energy gamma rays by the Milky Way interstellar radiation field, ApJ, 640, L155-L158, 2006.
- Moskalenko, I.V., Cosmic rays in the Milky Way and beyond, Nuclear Phys. B Proc. Suppl., 243, 85-91, 2013.
- Orlando, E. & Strong, A., Galactic synchrotron emission with cosmic ray propagation models, MNRAS, 436, 2127-2142, 2013.

- Paczynski, B., A test of the galactic origin of gamma-ray bursts, *ApJ*, 348, 485-494, 1990.
- Pierbattista, M., Grenier, I.A., Harding, A.K., & Gonthier, P.L., Constraining γ -ray pulsar gap models with a simulated pulsar population, *A&A*, 545, A42, 2012.
- Porter, T.A., Moskalenko, I.V., & Strong, A.W., Inverse Compton emission from Galactic supernova remnants: effect of the interstellar radiation field, *ApJ*, 648, L29-L32, 2006.
- Porter, T.A., Moskalenko, I.V., Strong, A.W., Orlando, E., & Bouchet, L., Inverse Compton origin of the hard X-ray and soft gamma-ray emission from the Galactic ridge, *ApJ*, 682, 400-407, 2008.
- Porter, T.A., Johnson, R.P., & Graham, P.W., Dark matter searches with astroparticle data, *Ann. Rev. Astron. Astrophys.*, 49, 155-194, 2011.
- Serpico, P.D., Astrophysical models for the origin of the positron “excess”, *Astropart. Phys.*, 39, 2-11, 2012.
- Schlickeiser, R., & Ruppel, J., Klein-Nishina steps in the energy spectrum of galactic cosmic-ray electrons, *New J. Phys.*, 12, 033044, 2010.
- Shaviv, N.J., Nakar, E., & Piran, T., Inhomogeneity in Cosmic Ray Sources as the Origin of the Electron Spectrum and the *PAMELA* Anomaly, *PRL*, 103, 111302, 2009.
- Spitkovsky, A., Time-dependent force-free pulsar magnetospheres: axisymmetric and oblique rotators, *ApJ*, 648, L51-L54, 2006.
- Story, S.A., Gonthier, P.L., & Harding, A.K., Population synthesis of radio and γ -ray millisecond pulsars from the Galactic disk, *ApJ*, 671, 713-726, 2007.
- Strauss, R.D., & Potgieter, M.S., Where does the heliospheric modulation of galactic cosmic rays start?, *Adv. Space Res.*, 53, 1015, 2014
- Strong, A.W., & Moskalenko, I.V., Propagation of cosmic-ray nucleons in the Galaxy, *ApJ*, 509, 212-228, 1998.
- Sturrock, P.A., A model of pulsars, *ApJ*, 164, 529-556, 1971.

- Venter, C., Harding, A.K., & Guillemot, L., Probing millisecond pulsar emission geometry using light curves from the *Fermi*/Large Area Telescope, *ApJ*, 707, 800-822, 2009.
- Venter, C., Kopp, A., Gonthier, P.L., Harding, A.K., & Büsching, I., Cosmic-ray positrons from millisecond pulsars, submitted to *ApJ*.
- Zhang, L., & Cheng, K.S., Cosmic-ray positrons from mature gamma-ray pulsars, *A&A*, 368, 1063-1070, 2001.

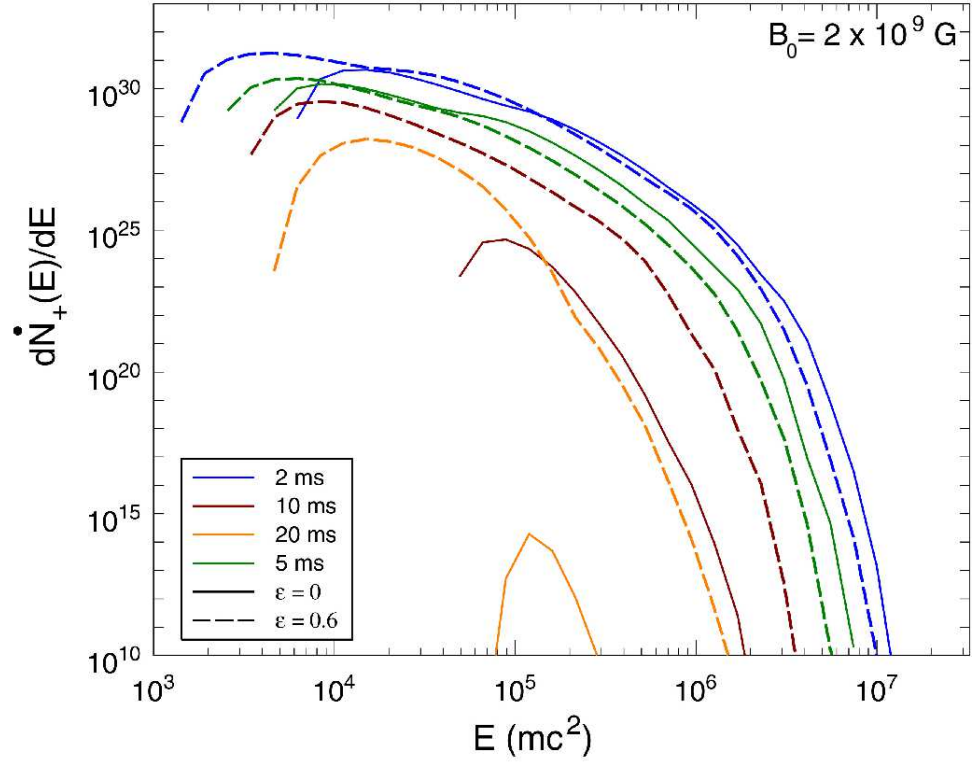


Figure 1: Sample electron-positron pair spectra (number of pairs per second and energy) calculated for different periods and offset values (P and ϵ), as indicated in the legend, and for a fixed value of $B_8 = 20$, i.e., $B_0 = 2 \times 10^9$ G. From [Harding & Muslimov \(2011\)](#).

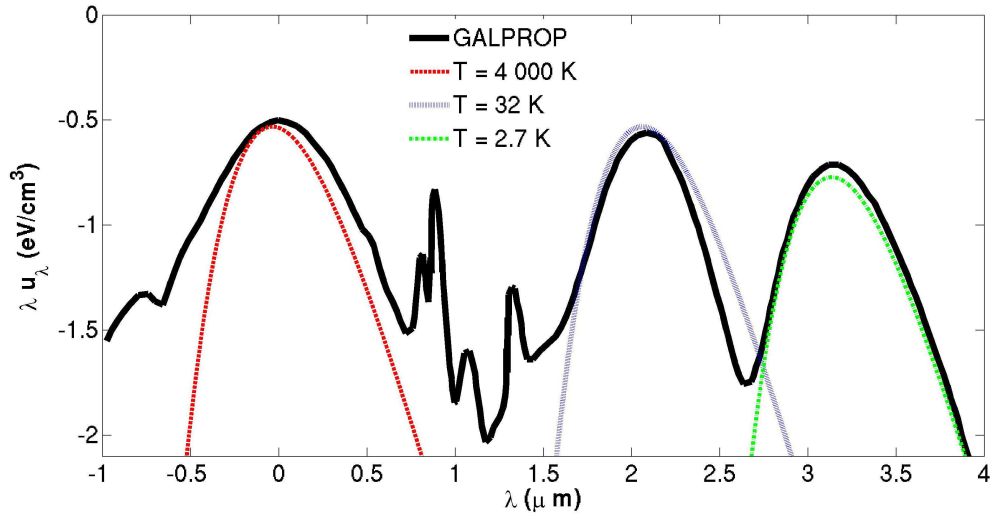


Figure 2: The ISRF as calculated by [Porter et al. \(2008\)](#) for the Galactic Plane, at a distance of 8 kpc from the Galactic Centre (thick black line), as well as three blackbody contributions which we use to approximate the ISRF (red dashed line: optical component with $T = 4000$ K; blue dotted line: IR component with $T = 32$ K; and green dashed-dotted line: CMB with $T = 2.7$ K). Our calculations make use of the average energy density of each component, and not of the temperatures *per se*.

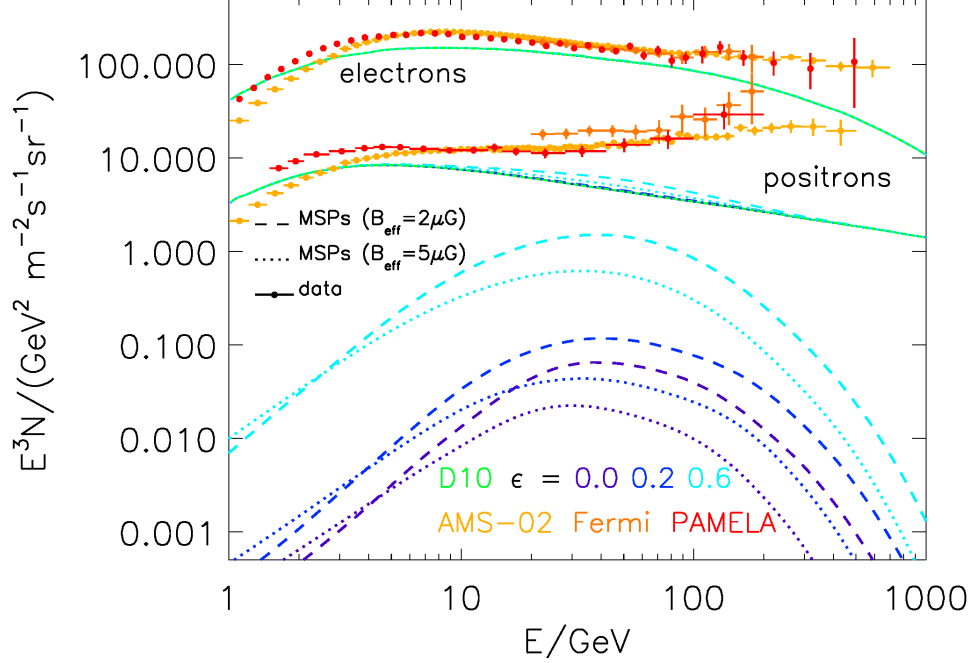


Figure 3: MSP contribution to the cosmic-ray lepton spectra at Earth. Electron spectra appear at the top, and positron spectra lower. The solid green lines indicate the “background” component of primary electrons from distant supernova remnants plus secondary electrons (upper solid line), as well as a component of secondary positrons (lower solid line) as predicted by D10. The hump-like primary MSP spectra (only positrons are shown, but the electrons are assumed to have identical spectra) appear at the bottom of the plot. From bottom to top (purple, blue, and cyan), these spectra are for $\varepsilon = 0.0, 0.2$, and 0.6 . The addition of the various MSP components to the background flux of D10 is indicated using the same colour convention. Dashed lines are for $B_{\text{eff}} = 2 \mu\text{G}$ and dotted lines for $B_{\text{eff}} = 5 \mu\text{G}$. Also shown are data from *PAMELA* (red; [Adriani et al., 2013](#)), *Fermi* (orange; [Ackermann et al., 2012](#)), and *AMS-02* (yellow; [Aguilar et al., 2014](#)), accessed via the website <http://lpsc.in2p3.fr/cosmic-rays-db> ([Maurin et al., 2014](#)).

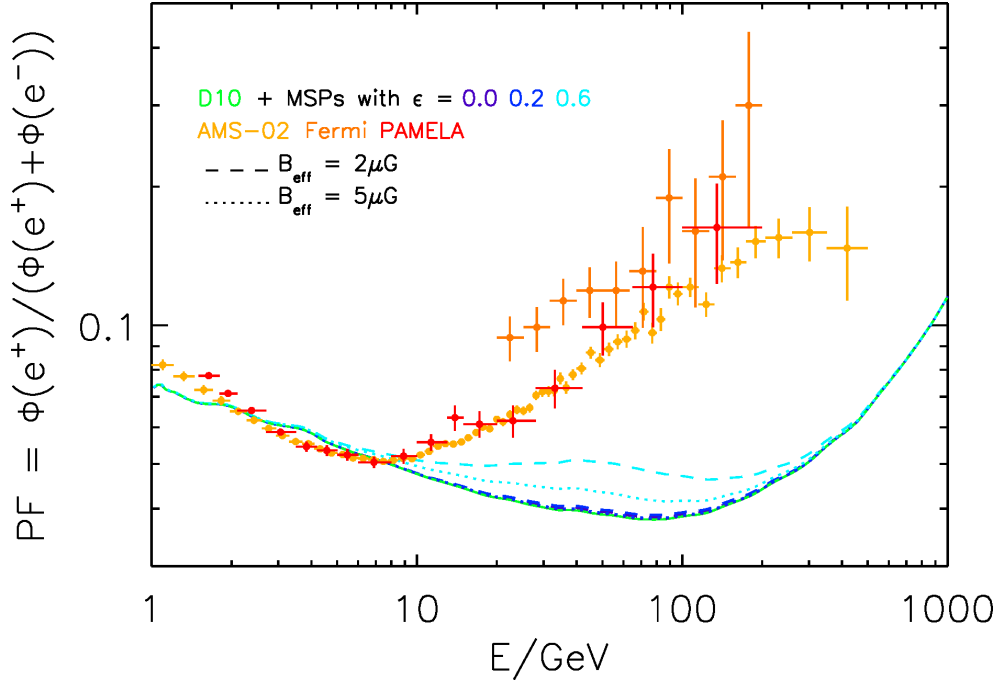


Figure 4: Measured ([Ackermann et al., 2012](#); [Adriani et al., 2013](#); [Accardo et al., 2014](#)) and predicted PF, including “background” contributions from D10 indicated by a solid green line, and the MSP contribution from this work. We use the same colour scheme and line styles as in Figure 3 to distinguish between values of ϵ and B_{eff} (see legend).